# Quantum simulation of bosonic-fermionic noninteracting particles in disordered systems via a quantum walk

Francesco De Nicola,[1] Linda Sansoni,[1,*] Andrea Crespi,[2,3] Roberta Ramponi,[2,3] Roberto Osellame,[2,3] Vittorio Giovannetti,[4] Rosario Fazio,[4,5] Paolo Mataloni,[1,6] and Fabio Sciarrino[1,6]

[1]*Dipartimento di Fisica, Sapienza Università di Roma, Piazzale Aldo Moro 5, I-00185 Roma, Italy*

[2]*Istituto di Fotonica e Nanotecnologie, Consiglio Nazionale delle Ricerche (IFN-CNR), Piazza Leonardo da Vinci 32, I-20133 Milano, Italy*

[3]*Dipartimento di Fisica, Politecnico di Milano, Piazza Leonardo da Vinci 32, I-20133 Milano, Italy*

[4]*NEST, Scuola Normale Superiore and Istituto di Nanoscienze–CNR, I-56126 Pisa, Italy*

[5]*Center for Quantum Technologies, National University of Singapore, 117542 Singapore, Singapore*

[6]*Istituto Nazionale di Ottica, Consiglio Nazionale delle Ricerche (INO-CNR), Largo Enrico Fermi 6, I-50125 Firenze, Italy*

(Received 16 December 2013; published 13 March 2014)

We report on the theoretical analysis of bosonic and fermionic noninteracting systems in a discrete two-particle quantum walk affected by different kinds of disorder. We considered up to 100-step quantum walks with a spatial, temporal, and spatial-temporal disorder observing how the randomness and the wave-function symmetry nontrivially affect the final spatial probability distribution, the transport properties, and the Shannon entropy of the walkers.

DOI: 10.1103/PhysRevA.89.032322 PACS number(s): 03.67.Ac, 42.50.−p

## I. INTRODUCTION

In statistical physics random walks describe the propagation of a particle (the walker) under the action of a probabilistic process which forces the latter to move along preassigned directions [say, one step on the left or one step on the right if the system is one dimensional (1D)]. Despite their simplicity, random walks have found applications in many research fields, spanning from economics to computer science, chemistry, and physics. A quantum version of this model was first provided by Aharonov, Davidovich, and Zagury [1], who introduced the notion of *quantum walks* (QWs).

Unlike their classical counterparts, in QWs, the final state of the walker is highly sensitive to the initial conditions of the system. Indeed, during its evolution, the particle spatial distribution does not converge to a steady state, but spreads ballistically. After a few steps, the counterintuitive profile of the wave function emerges as a result of quantum interference among many possible paths. The massive parallelism in exploring multiple trajectories is the basis for simulating biological [2,3], chemical [2], and physical [4–6] systems and is paving the way for universal quantum computation [7,8].

Regarding the experimental implementation of QWs, they have been observed in several scenarios, such as nuclear magnetic resonance [9], trapped ions and trapped cold neutral atoms [10–13], single photons in bulk [14], fiber optics [6,15,16], and coupled waveguide arrays [4,5,17–20]. The nature of the propagation of multiple particles in a QW may be strongly affected even in the absence of a direct interaction between them. Quantum (nonlocal) correlations present in the initial state will influence the overall wave-function evolution as the bunching or antibunching observed in interferometry. Entangled walkers have been studied both theoretically [14,17,21,22] and experimentally [4,5,23] in ordered and disordered systems. Depending on the symmetry of the input entangled state it is possible to simulate particles obeying different (boson or fermion) statistics.

With reference to the experimental realization of QWs in the presence of disorder presented in Ref. [23], here we report a detailed theoretical and numerical description of propagation of noninteracting bosonic and fermionic particles in a disordered environment. In this photonic approach, walkers are represented by photon pairs sharing polarization entanglement on a QW circuit implemented by an array of cascaded beam splitters, as we describe in the following. Generally, photons are limited to the behavior dictated by Bose-Einstein statistics, which defines quantum interference and quantum gates [24]. The ability to simulate nonbosonic statistics with photons by means of polarization entanglement could provide access to phenomena otherwise not physically accessible or that would be hidden by decoherence, providing a way to verify quantum simulations performed in other quantum systems [4,23,25]. Besides that, the controlled engineering of disorder would enable a detailed understanding of the distinct signatures of statistics on the system localization dynamics [23].

This paper is organized as follows. In the first section we briefly review the discrete-time QW and the two-particle probability distributions for an ordered structure. In Secs. III–V we analyze different types of disorder and the effects introduced into the walk by varying the symmetry of the input states. In Sec. VI, we investigate how the disorder strength affects the width of the wave packet, showing how the amount of disorder in the system can be varied in a controlled fashion. Fractality, anomalous diffusion, and other transport properties of bosonic and fermionic particles are discussed in Sec. VII, while Shannon entropy and mutual information of these states are reported in Sec. VIII. Section IX is devoted to the conclusions.

## II. DISCRETE-TIME QUANTUM WALK

Let us give a brief review of some basic concepts of the discrete-time QW. A quantum walker is a quantum

*linda.sansoni@gmail.com

 

particle—such as an electron, an atom, or a photon—characterized by both "external" and "internal" degrees of freedom, the former describing the propagation of the system in real space and the latter describing the state of the "coin" that dictates which path the particle has to follow during evolution. Accordingly, restricting ourselves to walks along a discrete 1D lattice, the generic state of the system can be expressed as

$$|\Psi\rangle = \sum_x |\psi(x)\rangle \otimes |x\rangle, \tag{1}$$

$$|\psi(x)\rangle = \alpha(x)|L\rangle + \beta(x)|R\rangle\ , \tag{2}$$

where $|x\rangle$ defines the particle position, with $\{|L\rangle, |R\rangle\}$ an orthonormal basis for the coin space (assumed hereafter to be bidimensional), and where $\alpha(x)$ and $\beta(x)$ are complex amplitudes (the probability of finding the particle at position $x$ irrespective of its internal state being $P(x) = |\langle x|\psi(x)\rangle|^2$ [26]). In this setting the dynamics is described as a stroboscopic process which, after $t$ steps, brings the generic initial state $|\Psi\rangle$ into the state

$$|\Psi(t)\rangle = \sum_x |\psi(x,t)\rangle \otimes |x\rangle = \hat{U}^t|\Psi\rangle, \tag{3}$$

with $\hat{U} = \hat{S}\cdot(\hat{C}\otimes\hat{I})$ being the unitary transformation obtained by first performing a Hadamard transformation $\hat{C}$ (coin) on the internal degree of freedom (with $\hat{I}$ corresponding to the identity operator), followed by a conditional displacement operator $\hat{S}$ [27]; i.e.,

$$\hat{C} = \frac{1}{\sqrt{2}}\begin{pmatrix} 1 & 1 \\ 1 & -1 \end{pmatrix}, \tag{4}$$

$$\hat{S} = \sum_x |L\rangle\langle L| \otimes |x-1\rangle\langle x| + |R\rangle\langle R| \otimes |x+1\rangle\langle x|. \tag{5}$$

Assume, hence, that the quantum walker is initially localized at position $x = 0$ with internal state $|L\rangle$ or $|R\rangle$. As a result of quantum interference among multiple paths that originates from $t$ steps of the evolution, (3), the counterintuitive profile of the QW probability distribution can be retrieved by measuring the position of the particle along the 1D line irrespective of its internal state, i.e., by looking at the quantity $P(x;t) = |\langle x|\psi(x,t)\rangle|^2$.

More complex probability distributions arise when two or more particles are injected into the same QW. In particular, an interesting situation is given by the evolution of identical particles obeying bosonic or fermionic statistics. In this case, due to the symmetrization postulate of quantum mechanics, bunching or antibunching is expected to influence the dynamics of the QWs. These effects have been analyzed by exploiting all-optical implementations of the discrete QW dynamics, (3) [4,23]. In these setups, built up from the theoretical proposals in Refs. [28,29], the propagation of a single quantum walker along a 1D line is simulated with a single photon which undergoes multiple scattering from 50:50 beam splitters organized in a bidimensional cascade array (see Fig. 1).

This is particularly convenient since the conditional displacement, (5), is automatically implemented (via a dual-rail encoding based on a "which-path" information) in the propagation along the network. Most interestingly, in these systems it is possible to emulate statistical effects associated with the evolution of two indistinguishable particles, by

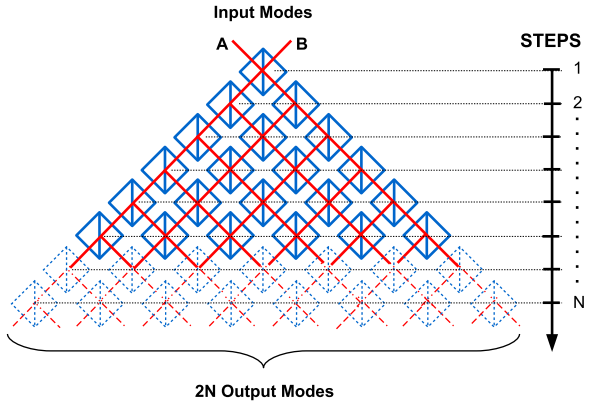


FIG. 1. (Color online) Photonic implementation of a 1D discrete-time quantum walk (QW). Each site is represented by a beam splitter [open (blue) squares]: a photon impinging on a symmetric beam splitter has the same probability of emerging from one of its two outputs. Due to this feature, the beam splitter may be used in a QW as both coin and step operator: by arranging many beam splitters in a cascaded configuration, it is possible to simulate an $N$-step QW circuit in which each line of beam splitters simulates a step in the QW [4,23].

exploiting the polarization degree of freedom of a couple of photons to enforce the proper symmetric or antisymmetric distributions on the effective 1D line [4,21,23]. Specifically, the QW of a pair of bosonic (fermionic) particles is obtained by injecting into the system the symmetric (antisymmetric) state $|\Psi^{(\pm)}\rangle$, defined by

$$|\Psi^{(\pm)}\rangle = \frac{1}{\sqrt{2}}\left(|\psi_A,H\rangle|\psi_B,V\rangle \pm |\psi_B,H\rangle|\psi_A,V\rangle\right), \tag{6}$$

where $|\psi_A,H\rangle = |\psi_A\rangle\otimes|H\rangle$ and $|\psi_B,H\rangle = |\psi_B\rangle\otimes|H\rangle$ are orthonormal vectors describing, respectively, a photon with horizontal polarization which is entering the array from two distinct ports of the setup (Fig. 1) (similar definitions apply for $|\psi_{A,B},V\rangle$ associated with a vertically polarized single photon). Assuming that the propagation through the network is polarization insensitive and that no interaction is present among the two photons, after $t$ steps Eq. (6) will evolve into

$$|\Psi^{(\pm)}(t)\rangle = \frac{1}{\sqrt{2}}\left[|\psi_A(t),H\rangle|\psi_B(t),V\rangle \pm |\psi_B(t),H\rangle|\psi_A(t),V\rangle\right], \tag{7}$$

where for $C = A,B$, $|\psi_C(t)\rangle = U^t|\psi_C\rangle$ is the evolved counterpart of the input state $|\psi_C\rangle$. Figure 2 reports the joint probability distribution $P^{(\pm,\mathrm{sym})}(x,y,t)$ associated with the detection of a photon in position $x$ and the other in position $y$, irrespective of their polarization, computed at $t = 50$ and assuming that $A$ and $B$ are two neighboring input ports in the setup [see Eq. (A8) in the Appendix for a formal definition of this quantity]. The different effects of symmetric ($P^{(+,\mathrm{sym})}$) and antisymmetric ($P^{(-,\mathrm{sym})}$) distributions, which can be related to bosonic and fermionic statistics, respectively, are shown in the corresponding probability distributions and density plots. The antibunching feature in Figs. 2(b) and 2(d) exhibits zero-probability diagonal elements, meaning that fermions are nontrivially arranged in space [4,22]. Most significantly, this pattern survives the random scattering process even after

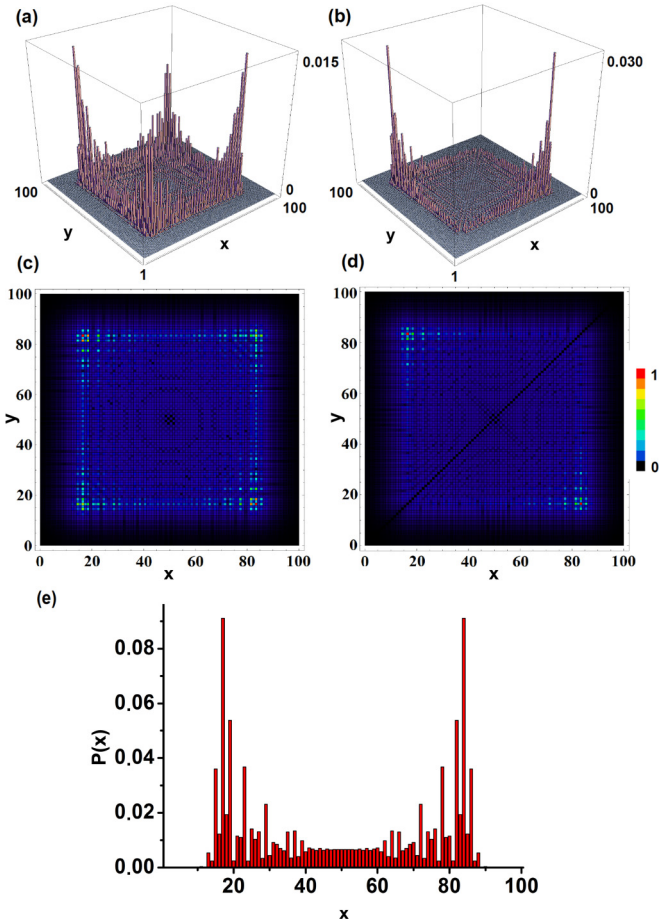


FIG. 2. (Color online) (a), (b) Mode probability distributions $P^{(\pm,\mathrm{sym})}(x,y,t)$ and (c), (d) associated density plots of bosonic (left) and fermionic (right) two-particle states. At $t = 0$, two particles are placed at two neighboring sites in the center of the lattice. The distribution is calculated after $t = 50$ steps. The matrices represent the probability of finding one particle at position $x$ and one at position $y$. Both bosons and fermions diffuse ballistically, giving rise to significant contributions in the corners of the probability distributions. Similar plots, but for $N = 30$ steps, can be found in Ref. [21]. (e) Marginal distribution $P^{\mathrm{sym}}(x)$ of Eq. (A10) obtained by summing over the columns in (c) and (d). The same distribution arises from both symmetric and antisymmetric distributions (see the Appendix).

very long evolution times. While bosons have a nonvanishing probability of bunching, fermions have zero probability of being at the same site, due to the Pauli exclusion principle [24,25]. This profound difference between the two QWs is a signature of the probability distribution's sensitivity to the initial state, due to the unitarity of the evolution.

## III. STATIC DISORDER AND ANDERSON LOCALIZATION

Let us now move to the description of such a scenario in the presence of disorder. Disorder exists at different levels in nature, ranging from a few impurities or interstitial defects in an otherwise perfect crystalline host [30–32] to the strongly disordered limit of glass structures [33]. In particular, the static disorder is set when a system parameter is a random variable evolving in space but not in time [34].

As predicted by Anderson, static disorder may lead to the absence of diffusion and the particle wave-function becomes localized [31]. This phenomenon, known as *Anderson localization*, has a fundamental relevance since it offers a mechanism to understand, for example, the electronic conductance in imperfect crystals and the metal-insulator transition [30,32,33]. The key factor for the interference effect responsible for the localization is the broken periodicity in the dynamics of the system, induced by the disordered media: random perturbations to the dynamics of the system can break the periodicity and manifest localization [15,35]. For 1D systems it can be rigorously shown that all states are localized because of the repeated backscattering, and the localization length is proportional to the mean free path of the particle, no matter how strong or weak the disorder is [32].

In the QW scenario localization may be controlled by introducing drifts with a constant momentum between two consecutive steps of the walk, i.e., by applying controlled phase-shift operations on the particle wave function to randomly stop at each site the evolution of the quantum coin [36], whose matrix now reads

$$C(x,t) = C(x) = \frac{1}{\sqrt{2}} \begin{pmatrix} e^{i\phi_L(x)} & 0 \\ 0 & e^{i\phi_R(x)} \end{pmatrix} \begin{pmatrix} 1 & 1 \\ 1 & -1 \end{pmatrix}. \quad (8)$$

At each step, coin operations evolve the initial state by applying the same phases $\{\phi_L(x), \phi_R(x)\}$. While in the absence of disorder the QW exhibits a spatial probability distribution diffusing ballistically, in the case of static disorder the distribution appears to be localized, with a shape characterized by an exponential decay.

Single-particle transport in disordered lattices has been experimentally observed in different frameworks (microwaves in strongly scattering samples [37], single photons in bulk [38], photonic lattices [39], ultrasound waves in a 3D elastic system [40], and Bose-Einstein condensates [41]); conversely, there are few numerical studies [6,22] and only two experiments on multiparticle transport [23,42].

Understanding the behavior of a multiparticle system in a disordered medium may be of great interest. Indeed, the bosonic or fermionic nature of the particles strongly affects the transport phenomenon, deriving from both wave interference and quantum correlations. Because of the coin operation's unitarity, the static disorder only affects the shape of the distribution and does not alter the symmetry of the initial state. Therefore the QW with static disorder still proves strongly dependent on the input state, as the antibunching feature shows with the diagonal-vanishing pattern in Fig. 3(d).

By tracing out the position of one of the particles [i.e., summing over the columns of the correlation matrix as detailed in Eq. (A10)], it is possible to confirm the exponential decay of the Anderson peak by computing the linear fit of the distribution on a semilogarithmic scale [Figs. 3(e) and 3(f)] and therefore calculating the localization length in inverse proportion to the angular coefficient.

The analysis reported here, dealing with a discrete-time QW, could also beperformed by exploiting a continuous-time QW; indeed, the two approaches have shown many similarities [43]. Simulations of space-dependent disorder for two-particle systems have been reported in this case by Lahini *et al.* [22],

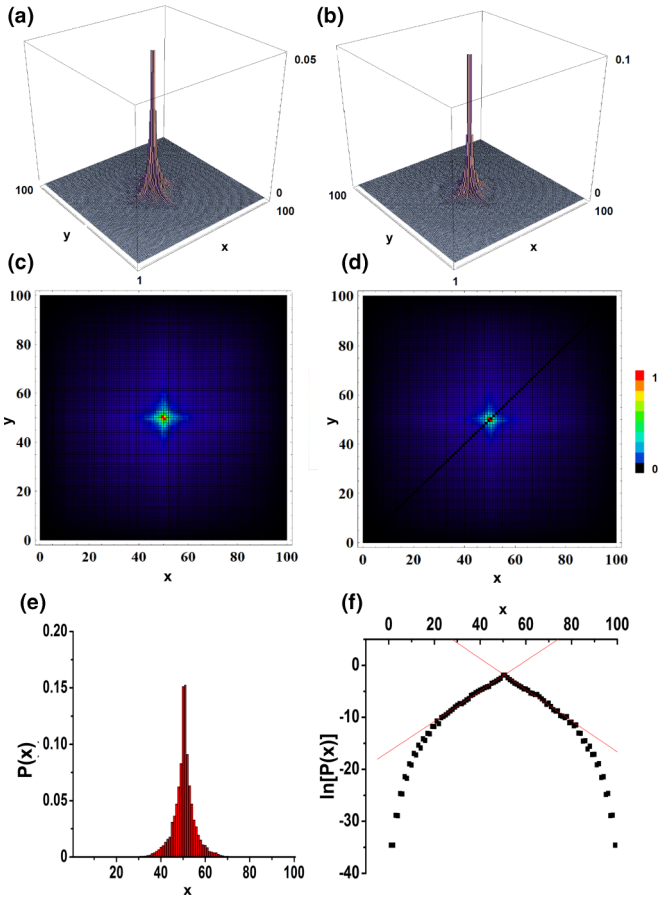


FIG. 3. (Color online) (a), (b) Mode probability distributions $P^{(\pm,\mathrm{sym})}(x,y,t)$ and (c), (d) associated density plots of bosonic (left) and fermionic (right) two-particle states in the case of a quantum walk in the presence of static disorder. At $t = 0$, two particles are placed at two neighboring sites in the center of the lattice. The distribution is calculated after $t = 50$ steps and averaged over 100 configurations of static disorder. Both bosons and fermions localize near their initial position, with a typical distribution profile characterized by an exponential decay. The dependence on the symmetry of the initial state is still observable. (e) Marginal distribution $P^{\mathrm{sym}}(x)$ of Eq. (A10) obtained by summing over the columns in (c) and (d). (f) Linear fit on a semilog scale. The localization length after 50 steps of a two-particle quantum walk is estimated to be $\xi \cong 3$.

where the two-particle correlation function is calculated after short evolution times, in such a way that each particle has nonzero probability of being localized or remaining ballistic: it may be associated with an evolution in the presence of static disorder whose strength (see Sec. VI) is nonmaximal. At variance with this approach, in our scenario we implement a maximal-strength static disorder. In this case the probability of the particles diffusing ballistically becomes negligible on a 100-step QW, allowing us to observe a pure localization effect.

## IV. SPACE-CORRELATED DYNAMIC DISORDER AND DECOHERENCE

In this section we consider the case of a two-particle QW in the space-correlated dynamic disorder simulating the transition from QW to classical random walk for bosons and fermions. The evolution is related to the degrees of freedom defining the system such as external fields, temperature, pressure, and doping [34]. By turning on an interaction between the quantum system and the environment, the fluctuations in the environment lead to a reduction in the coherence in the quantum system. This is the cost of extracting knowledge about the state of a system [44]. Thus decoherence plays a crucial role in the transition from quantum to classical world. The controlled introduction of decoherence enables a detailed comprehension of its effects on the system dynamics, enabling the simulation of biological phenomena which exploit these features [2].

The impact of decoherence on QWs has been investigated both numerically and experimentally, in various settings, mostly in 1D systems [15,23,44] using repeated measurements [27,44,45] or topological noise by quantum coin phase-shift operations [15,23,35,44]. In this case the time-dependent coin operator reads

$$C(x,t) = C(t) = \frac{1}{\sqrt{2}} \begin{pmatrix} e^{i\phi_L(t)} & 0 \\ 0 & e^{i\phi_R(t)} \end{pmatrix} \begin{pmatrix} 1 & 1 \\ 1 & -1 \end{pmatrix}. \quad (9)$$

By assigning different quantum coin operators at every step of the walk while retaining the same at each spatial site $[\phi_L(t) = \phi_R(t)]$, thus eliminating position-dependent phase correlations, the complete evolution will be expressed as $C(t)C(t-1)\ldots C(2)C(1)$ [6,35]. Decoherence appears as a consequence of the dynamically varying phase suffered by the quantum particle during its evolution. As a result, the photon undergoes a classical random walk, revealing a binomial probability distribution [15,44]. In contrast to the previous case, the spatial profile of the wave packet in Fig. 4(f) shows a parabolic shape on the semilog scale, confirming a Gaussian distribution profile as expected for classical systems.

It is important to highlight that, even with the introduction of decoherence in QWs by quantum coin phase-shift operations, the system dynamics is still unitary because the phase-shift operator is unitary. Hence decoherence is caused only by an interference effect that mixes the position distribution of the QW to a uniform distribution essentially as in the classical case. Therefore, in the presence of dynamic disorder the QW is still strongly dependent on the symmetry of the input state. Quantum particles lose their quantum waveform but not their quantum properties, giving rise to a classical particle distribution profile exhibiting wave-particle dualism.

## V. UNCORRELATED DYNAMIC DISORDER AND ANDERSON TRANSITION

As shown in Sec. III, a particle moving in a spatially disordered time-independent potential can exhibit Anderson localization. At the same time, it is known that, if the disordered potential is also fluctuating in time, localization is lost and transport is restored. This is the so-called Anderson transition, observed under a great variety of experimental conditions, from electromagnetic waves propagating in strongly disordered dielectric structures such as doped semiconductors and amorphous systems [30–33]. This transition can be obtained by changing the temperature, pressure, doping [32], or

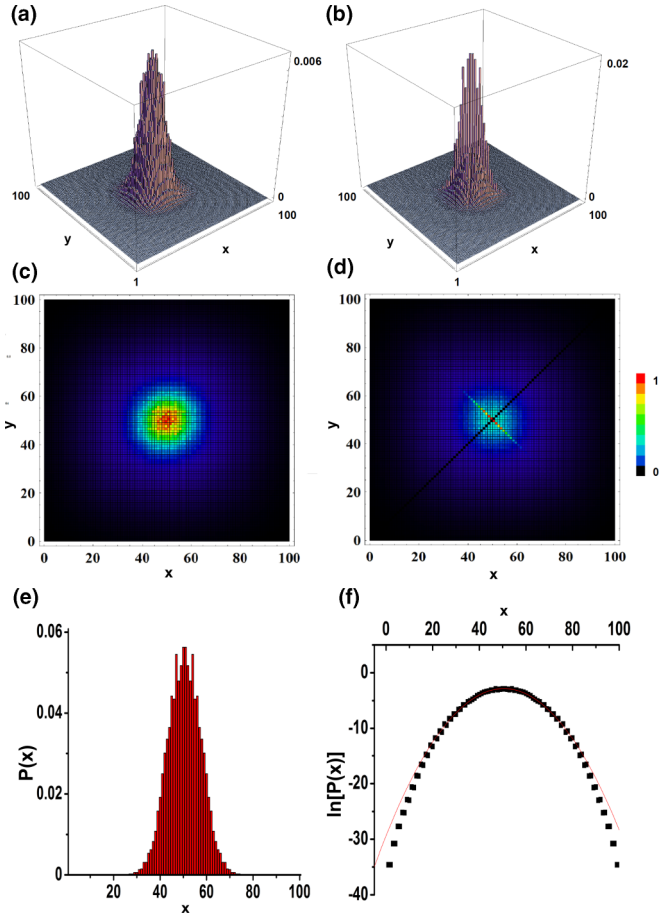


FIG. 4. (Color online) (a), (b) Mode probability distributions $P^{(\pm,\mathrm{sym})}(x,y,t)$ and (c), (d) associated density plots of bosonic (left) and fermionic (right) two-particle states in the case of dynamic disorder. At $t = 0$, two particles are placed at two neighboring sites in the center of the lattice. The distribution is calculated after $t = 50$ steps and averaged over 100 configurations of dynamic disorder. Both bosons and fermions localize near their initial position, with a typical binomial distribution profile characteristic of a classical random walk, but the dependence on the symmetry of the initial state is still observable. (e) Marginal distribution $P^{\mathrm{sym}}(x)$ of Eq. (A10) obtained by summing over the columns in (c) and (d). (f) Parabolic fit on the semilog scale.

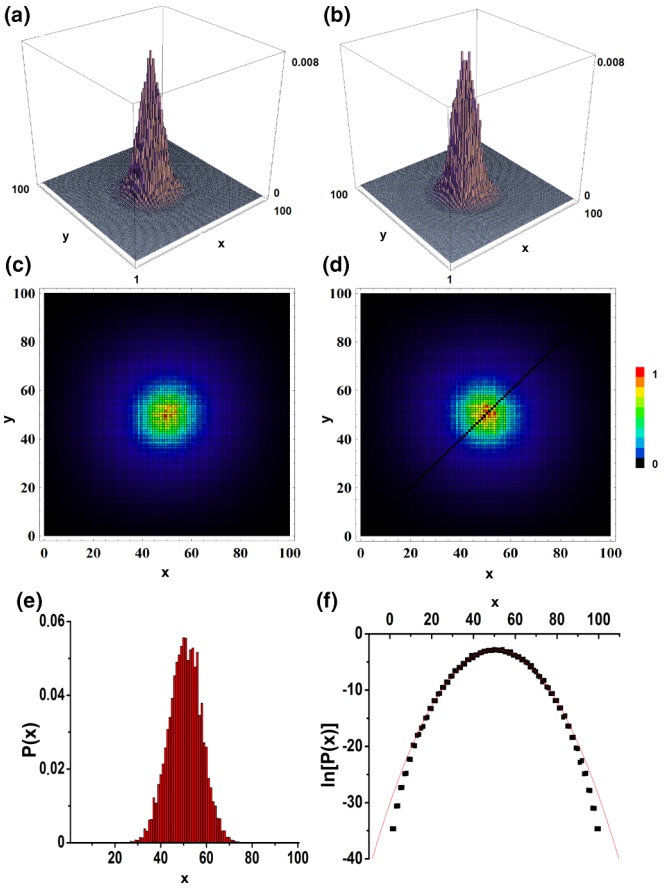


FIG. 5. (Color online) (a), (b) Mode probability distributions $P^{(\pm,\mathrm{sym})}(x,y,t)$ and (c), (d) associated density plots of bosonic (left) and fermionic (right) two-particle states in the case of fluctuating disorder. At $t = 0$, two particles are placed at two neighboring sites in the center of the lattice. The distribution is calculated after $t = 50$ steps and averaged over 100 configurations of disorder. Space-correlated dynamic disorder competes with static disorder, extending quantum states and forbidding localization. The result is that both boson and fermion distributions become Gaussian and the dependence on the symmetry of the initial states remains. (e) Marginal distribution $P^{\mathrm{sym}}(x)$ of Eq. (A10) obtained by summing over the columns in (c) and (d). (f) Parabolic fits on a semilog scale.

magnetization [33]. Over the years, several mechanisms have been proposed for the breakdown of Anderson localization due to temporal fluctuations of the potential [46–48]. Mott considered the effect of phonons at low temperatures and argued that this gives rise to a diffusive motion known as *variable-range hopping conductivity*. Mott also considered the effects of a weak ac field and suggested that a resonant interaction dominates the low-frequency response [32,48].

By combining the two previous disordered scenarios, we may simulate a symmetric or an antisymmetric system in which localized states become extended states with time due to decoherence effects. By randomly assigning different quantum coin operators for each lattice site and changing these operators during each step of the evolution, we induce a spatiotemporal disorder or *fluctuating disorder* [35]. Therefore the quantum coin operator of the $t$th step of the dynamics can be expressed as

$$C(x,t) = \frac{1}{\sqrt{2}} \begin{pmatrix} e^{i\phi_L(x,t)} & 0 \\ 0 & e^{i\phi_R(x,t)} \end{pmatrix} \begin{pmatrix} 1 & 1 \\ 1 & -1 \end{pmatrix}, \qquad (10)$$

where the value of $\phi_{L,R}(x,t)$ is randomly chosen at every step $t$ and at each site $x$. Thus the complete evolution of the walk will be given by $C(x,t)C(x,t-1)\ldots C(x,2)C(x,1)$ [35].

This scenario leads to distributions similar to those obtained in the presence of space-correlated dynamic disorder (compare Figs. 4 and 5); however, Fig. 5 shows that with an increasing number of steps the dynamic variation of the phase competes with the localization effect given by the static variation of the phase, displaying a Gaussian probability distribution. In the space-correlated dynamic disordered scenario, we have shown that particles started in a disorder-free configuration with extended distributions of quantum states and the effect of disorder was to shrink the wave functions displaying

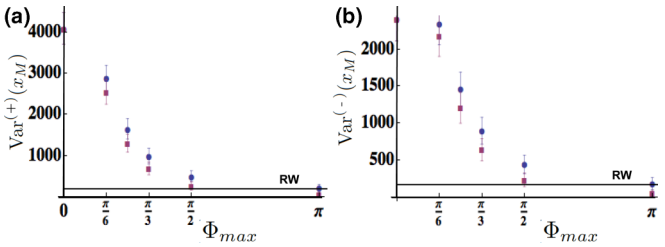


FIG. 6. (Color online) Transition of the mean position variance $\mathrm{Var}^{(\pm)}(x_M)$ of Eq. (11) of symmetric (a) and antisymmetric (b) states from ballistic quantum walk to diffusive or subdiffusive evolution after 100 steps due to dynamic [(blue) circles] and static [(purple) squares] disorder with increasing disorder strength $\Phi_{\max}$ (measured in radiants). Each data point is averaged over 100 configurations of disorder and the error bars represent the standard deviation. The solid black line marks the variance of the classical random walk (RW).

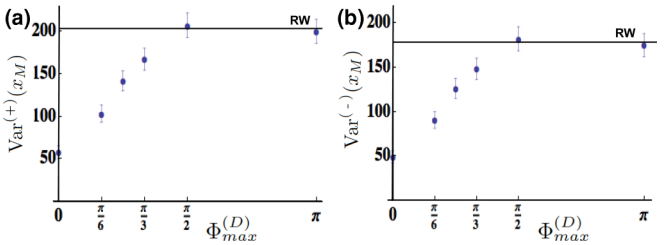


FIG. 7. (Color online) Transition of the mean position variance $\mathrm{Var}^{(\pm)}(x_M)$ of Eq. (11) of symmetric (a) and antisymmetric (b) states from subdiffusive quantum walk to diffusive evolution after 100 steps due to dynamic disorder [(blue) circles] with increasing dynamic disorder strength $\Phi^{(D)}_{\max}$ once the static disorder strength is fixed, $\Phi^{(S)}_{\max} = \pi$. The mobility edge is $\Phi^{(D)}_{\max} \cong \pi/2$ (all phases are given in radiants). Every data point is averaged over 100 configurations of disorder and the error bars represent the standard deviation. The solid black line marks the variance of the classical random walk (RW).

a Gaussian profile. Here, input states first localize in an Anderson peak owing to static disorder, and only after the distributions become binomial due to decoherence: static disorder has a priority on dynamic disorder because the former acts on different spatial sites in the same temporal step, while the latter's action is the same for all sites in a given step. This is well evident by comparing Figs. 4(d) and 5(d): the fermionic distribution in the latter case has a Gaussian spatial profile that is more pronounced and very similar to the bosonic wave packet, related to the fact that input states localize before becoming extended. Therefore, dynamic disorder is a global effect on the walk and it is slower than the static effect, as we show in the next section. Also in this case, the QW still has a strong dependence on the symmetry of the input state, as we can note in Fig. 5.

## VI. DISORDER STRENGTH

When a disordered scenario is considered, the degree of disorder needs to be characterized quantitatively. This physical quantity can be addressed by taking into account the disorder strength, which is determined by $\Phi_{\max}$, i.e., the maximal applied phase shift which defines the uniform interval $[0, \Phi_{\max}]$ from which $\{\phi_L(x), \phi_R(x)\}$ are randomly chosen [15].

The stepwise increase in the disorder strength $\Phi_{\max}$ enables the controlled transition of the system from the ballistic evolution of the disorder-free QW towards diffusive (subdiffusive) evolution in a scenario with dynamic (static) disorder, as shown in Fig. 6. To this purpose we characterized the resulting expansion profile by the two-particle distribution variance $\mathrm{Var}^{(\pm)}(x_M)$ of twice their mean position, $x_M = x + y$; i.e.,

$$\mathrm{Var}^{(\pm)}(x_M) = \sum_{x,y=1}^{N} (x+y)^2 P^{(\pm,\mathrm{sym})}(x,y) - \left[\sum_{x,y=1}^{N} (x+y) P^{(\pm,\mathrm{sym})}(x,y)\right]^2 . \quad (11)$$

Clearly, this quantity will result in different behaviors for the symmetric state (related to bosonic evolution) and the antisymmetric one (related to fermionic evolution), the exact connection with the particle statistics being detailed in Eq. (A12). Moreover, it will be strongly affected by the presence of disorder.

In Fig. 6 we report the variance, (11), calculated for 100-step QWs in the presence of static [(purple) squares] and space-dependent dynamic [(blue) circles] disorder, with different values of the maximum disorder strength, averaged on 100 random distributions. Without disorder ($\Phi_{\max} = 0$) the ballistically spreading wave packet shows a large expansion induced by quantum interference after 100 steps. In a system with dynamic disorder (circles), decoherence reduces the expansion of the wave packet to the level of a diffusive classical particle (solid black line).

On the contrary, static disorder (squares) leads to a stagnation of the spread due to the Anderson localization effect and hence an even smaller variance. The variance exponentially decreases as the disorder strength increases and, in general, as the number of steps grows. By comparing the two behaviors reported in Fig. 6, we may notice that the presence of static disorder tends to localize the distribution more rapidly than the space-correlated dynamic disorder since, for each value of disorder strength, the variance in the presence of space-dependent disorder is lower than the variance obtained in the dynamic-disordered scenario. We infer from Fig. 6(a) that the maximal localizing interval is $[0, \pi]$, irrespective of the particle statistics. This is the same interval we used in all the previous simulations. These results clearly demonstrate how the amount and kind of disorder influence the expansion of the particle wave packet.

Let us now consider the variance of a QW in the presence of uncorrelated dynamic disorder [(blue) circles in Fig. 7] and a stepwise increase in the dynamic disorder strength $\Phi^{(D)}_{\max}$ once the static disorder strength is fixed to its highest value, $\Phi^{(S)}_{\max} = \pi$. From Fig. 7 it is possible to rate the dynamic disorder strength necessary to extend the localized states and, in this way, realize a controlled Anderson transition. The mobility edge is defined as the critical value of disorder strength for which the variance reaches the level of a classical random walk (solid black line). For values of $\Phi^{D}_{\max}$ below the mobility edge the variance decreases because static disorder dominates, thus localizing the particle wave packet.

## VII. TRANSPORT PROPERTIES AND FRACTALITY

In this section we study how the transport properties of particles are connected to the fractality of the system. Fractals are mathematical objects with a Hausdorff-Besicovitch dimension which is not an integer [47,49]. Fractals are best constructed in a recursive way and their limiting curve is of infinite length, although it is confined to a finite region of the plane. The best way to characterize them is by using their fractal dimension $d$. When calculating this quantity we notice the striking property of self-similarity: every fractal curve is similar to the fractal curve of a part of itself, or, in other words, it is said to be a scale invariant.

Classical random walks are self-similar only in a statistical sense [47]. For these objects a fractal dimension $d$ is still easily defined by the scaling of their fractal mass $M$ with their linear size $L$, $M \approx L^d$. As a consequence, classical random walks are statistical fractals with Hausdorff dimension $d = 2$ [47]. Conversely, QWs are not fractals even in the statistical sense: because of their quantum nature, their fractal dimension is $d = 1$.

Particle transport in a lattice has been widely investigated in the framework of the QW [2,15,47]. One of the most important physical parameters describing a random walk is the mean-square displacement covered by the walker once it has passed through $t$ steps. This quantity is proportional to the variance of the center of mass of Eq. (11). In uniform Euclidean systems, the mean-square displacement of a random walker is proportional to the time, for any number of spatial dimensions agreeing with Fick's law [47]. Random walks describe the probabilistic evolution of a classical particle in a structured space resulting in a diffusive transport. In contrast, endowing the walker with quantum mechanical properties typically leads to a ballistic spread of the particle's wave function [15].

However, in disordered systems, Fick's law is not valid in general. Rather, we may recall the localization behavior as anomalous diffusion [47]: $\langle \mathbf{x}^2(t) \rangle \propto t^{\frac{2}{d}}$. Note that classical Fick diffusion with $d = 2$ can be considered anomalous diffusion with respect to the quantum case with $d = 1$.

The observed slowing-down of the transport is caused by the delay of the diffusing particles in the dangling ends, bottlenecks, and backbends existing in the disordered structure. Examples of disordered systems for which anomalous diffusion has been observed are percolation clusters [50,51], fractal lattices [47], and classical and quantum random walks [15,23].

In Fig. 8 we report step by step the variance $\mathrm{Var}^{(\pm)}(x_M)$ of Eq. (11) of the center of mass in all four of the previous QW scenarios (the disorder strength is maximum), for symmetric and antisymmetric input states. First, we note that, due to the symmetry of the states, bosons diffuse more rapidly than fermions, reaching higher variance values. Moreover, by computing the polynomial fits of these curves we obtain the correct trends of the mean-square displacement and the fractal dimensions, for the two-particle QW with bosonic and fermionic input states. In the disorder-free case the QW has fractal dimension $d \approx 1$; therefore the diffusion, characterized here by the positional probability distribution variance, is ballistic, $\mathrm{Var}^{(\pm)}(x_M,t) \propto t^2$ circles]. In the presence of dynamic and fluctuating disorder, the fractal dimension is

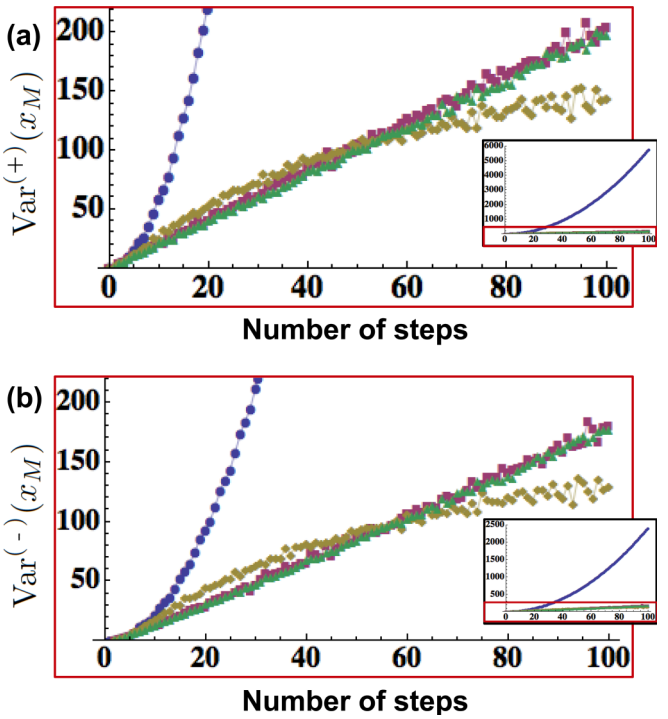


FIG. 8. (Color online) Trend of mean position variance $\mathrm{Var}^{(\pm)}(x_M)$ of Eq. (11) up to 100 steps of a bosonic (a) and a fermionic (b) quantum walk in different scenarios. For the disorder-free case [(blue) circles] we observe a ballistic spread (full behavior shown in insets). The evolutions with space-correlated dynamic [(purple) squares] and uncorrelated [(green) triangles] disorder are clearly diffusive. Finally, under the condition of static disorder [(yellow) diamonds] the variance starts to saturate after a few steps and the dynamics shows the onset of Anderson localization. The parameters used in this simulation are equivalent to the simulation settings used for Figs. 2–5. Each data point for the four kinds of disordered quantum walks is averaged over 100 configurations of disorder. Error bars have been omitted for clarity.

$d \approx 2$, therefore the motion is diffusive, $\mathrm{Var}^{(\pm)}(x_M,t) \propto t$ [(purple) squares and (green) triangles]. Finally, in the case of the static disordered QW the fractal dimension is $d \approx 3.4$ and the trend is subdiffusive, $\mathrm{Var}^{(\pm)}(x_M,t) \propto t^{0.6}$, thus leading to particle stagnation [(yellow) diamonds].

## VIII. SHANNON ENTROPY AND MUTUAL INFORMATION

An alternative method to measure the position fluctuation with the variance is provided by the joint Shannon entropy of the two walkers' position probability distribution $P^{(\pm,\mathrm{sym})}(x,y)$, which, via Eq. (11), describes the statistics in the bosonic (fermionic) case. This is

$$H(X,Y) \equiv -\sum_{x,y} P^{(\pm,\mathrm{sym})}(x,y) \log_2 P^{(\pm,\mathrm{sym})}(x,y). \quad (12)$$

This quantity varies with the number of steps in a similar way for symmetric and antisymmetric particles, however, the values of $H(X,Y)$ obtained at each step depend on the particle statistics. In particular, we may observe in Fig. 9 that the distribution $P^{(-,\mathrm{sym})}(x,y)$ (dashed line) shares a joint entropy lower than the one shared by the distribution $P^{(+,\mathrm{sym})}(x,y)$

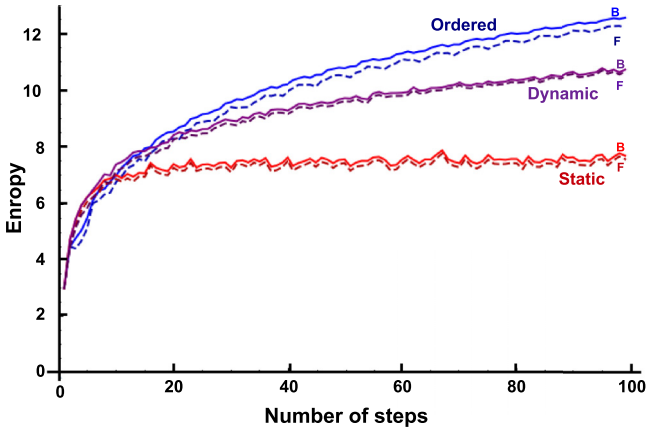


FIG. 9. (Color online) Joint Shannon entropy, (12), up to 100 steps of symmetric (solid curves) and antisymmetric (dashed curves) quantum walks under different conditions. We may observe how the increase in entropy is slowed when passing from the ordered [upper (blue) curves] to the disordered case, saturating in the case of static disorder [lower (red) curves]. For each type of disorder the entropy of the $P^{(-,\mathrm{sym})}(x,y)$ distribution is always lower than the entropy of $P^{(+,\mathrm{sym})}(x,y)$. Each data point for the three kinds of disordered quantum walks is averaged over 50 configurations of disorder. Error bars have been omitted for clarity.

(solid line), and this happens in the presence of any kind of disorder. The Shannon entropy, which we may consider the amount of information gained by increasing the number of steps in the QW, depends on the type of disorder the walker undergoes during the walk.

As reported in Fig. 10 we also calculated another quantity, the mutual information. The mutual information content of $X$ and $Y$ measures the amount of common information about the spatial position of the two particles, and its expression reads

$$\begin{aligned} I^{(\pm)}(X:Y) &= H(X) + H(Y) - H^{(\pm)}(X,Y) \\ &= 2H(X) - H^{(\pm)}(X,Y), \end{aligned} \tag{13}$$

where $H$ is the Shannon entropy associated with the single-particle marginal, (A10) (note that it does not depend on the symmetry of the input state; see the Appendix).

We may observe in Fig. 10 that this quantity reaches an asymptotic value in the disorder-free case [upper (blue) curve] and in the presence of static disorder [middle (yellow) curve], while it slowly decreases in the presence of dynamic disorder [lower (purple) curve]. In the presence of this type of disorder, indeed, the distribution tends to the classical one, so we may imagine that one particle loses information about the position of the other one since they tend to behave like independent walkers. Both the symmetric and the antisymmetric distributions exhibit this behavior, however, symmetric particle systems share a mutual information lower than the one shared by antisymmetric particles. This may be naively understood by observing that, since the antisymmetric distribution is related to fermionic behavior, due to the Pauli exclusion principle, fermions cannot occupy all possible two-particle positions: this corresponds to a residual mutual knowledge between the two walkers. For the same reason, it is expected that the higher residual correlation occurring in the antisymmetric

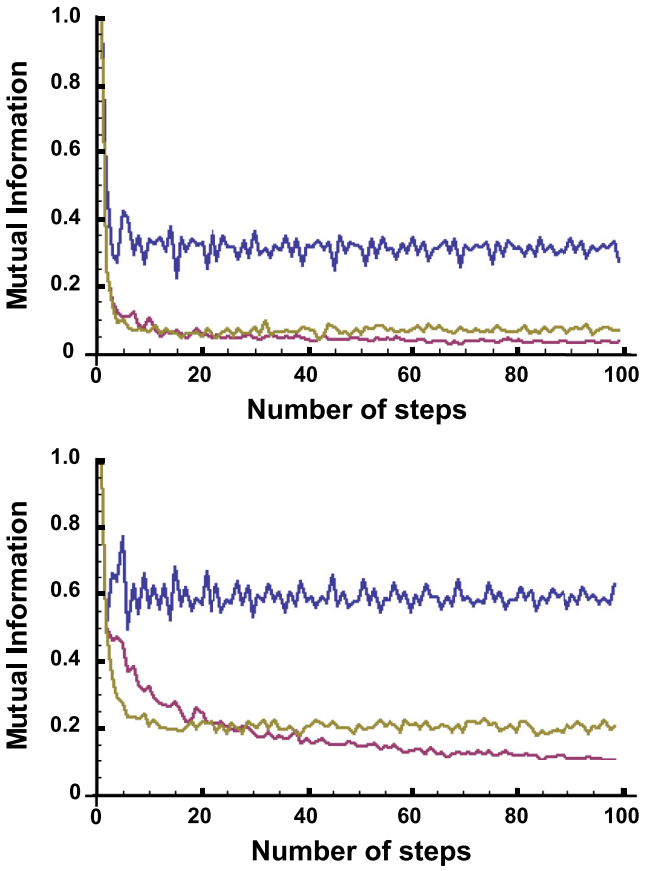


FIG. 10. (Color online) Mutual information, (13), up to 100 steps of the quantum walk for (a) the distribution $P^{(+,\mathrm{sym})}(x,y)$ and (b) the distribution $P^{(-,\mathrm{sym})}(x,y)$ in the disorder-free case [upper (blue) line], dynamic disordered case [lower (purple) line], and static disordered case [middle (yellow) line]. Mutual information decreases as the number of steps increases. At each step the mutual information for bosons is lower than that for fermions. Each data point for the three kinds of disordered quantum walks is averaged over 50 configurations of disorder. Error bars have been omitted for clarity.

case, compared to the symmetric one, survives even in the limit of an infinite number of steps, since the particle statistics is not affected during the walk. This is enforced by observing from Eq. (13) that the difference in the mutual information between symmetric and antisymmetric systems arises only from the difference between the corresponding joint Shannon entropies; indeed the marginal entropies [$H(X)$ and $H(Y)$] do not depend on the particle statistics. Thus a brief look at Fig. 9 confirms that the gap in entropies between symmetric and antisymmetric systems does not decrease as the number of steps increases.

## IX. CONCLUSIONS

In this paper, we have presented a theoretical analysis of two noninteracting bosons and fermions traveling in a discrete-time QW. By varying the parameters of the system, transport properties have been studied. Then the interplay between quantum coherence and the presence of

dephasing disorder has been investigated, with particular attention to entanglement and disorder-assisted transport effects. By introducing suitable static disorder into the walk we have simulated the absence of diffusion in a periodic lattice. Under these conditions, the onset of Anderson localization has been observed. Furthermore, decoherence deriving from dynamic disorder has been investigated, simulating the transition between the quantum and the classical worlds. Finally, we have presented how fluctuating disorder can lead to a deeper comprehension of the Anderson transition.


## ACKNOWLEDGMENT

This project was supported by FIRB–Futuro in Ricerca HYTEQ, PRIN 2009, and ERC 3D-QUEST.


## APPENDIX: POLARIZATION AND STATISTICS

Given state (7), the probability of detecting one photon in position $x$ and the other in position $y$, irrespective of their polarization, is written

$$P^{(\pm)}(x,y,t)=\begin{cases}|\langle x,H|\langle y,V|\Psi^{(\pm)}(t)\rangle|^2+|\langle y,V|\langle x,H|\Psi^{(\pm)}(t)\rangle|^2, & i>j,\\ |\langle x,H|\langle x,V|\Psi^{(\pm)}(t)\rangle|^2, & x=y,\end{cases} \tag{A1}$$

where $|x,H\rangle$ and $|x,V\rangle$ describe a photon emerging from the output port $x$ of the setup with horizontal and vertical polarization, respectively. Explicitly, this is

$$P^{(\pm)}(x,y,t)=\begin{cases}|\psi_A(x,t)\psi_B(y,t)\pm\psi_A(x,t)\psi_B(y,t)|^2 & \text{for}\quad x>y,\\ \begin{cases}2\,|\psi_A(x,t)\psi_B(y,t)|^2 & \text{for}\quad (+),\\ 0 & \text{for}\quad (-),\end{cases} & \text{for}\quad x=y,\end{cases} \tag{A2}$$

where for $C=A,B$ we have introduced the single-particle amplitude probabilities,

$$\psi_C(x,t)=\langle x|\psi_C(t)\rangle. \tag{A3}$$

[We stress that to avoid double-counting, $P^{(\pm)}(x,y,t)$ is defined *only* for $x\geqslant y$.]

The probabilities defined above correspond to the probabilities one would get if the particles were indistinguishable and obeyed bosonic or fermionic statistics. This is a consequence of two facts: (i) while in Eq. (7) the two particles are distinguishable in terms of their polarization degrees of freedom, the measurement we consider is transparent with respect to this degree of freedom (we do not distinguish whether the emerging photon is $H$ or $V$); and (ii) the vector $|\Psi^{(\pm)}\rangle$ is symmetric (antisymmetric) for particle (i.e., polarization) exchange. To see this explicitly observe that in the first quantization, having identified the polarization with the particle indexes, we have that $|\Psi^{(+)}(t)\rangle$ defines a proper state of two bosons. The probability of detecting one of the two particles in position $x$ and the other in $y$ ($<x$) can then be obtained by projecting $|\Psi^{(+)}(t)\rangle$ in the bosonic state which represents this final configuration [i.e., the symmetric vector $(|x,H\rangle|y,V\rangle+|y,H\rangle|x,V\rangle)/\sqrt{2}$)],

$$\begin{aligned}P^{(\mathrm{BOS})}(x,y)&=\left|\left[\frac{\langle x,H|\langle y,V|+\langle y,H|\langle x,V|}{\sqrt{2}}\right]|\Psi^{(+)}\rangle\right|^2\\&=|\psi_A(x)\psi_B(y)+\psi_A(x)\psi_B(x)|^2=P^{(+)}(x,y),\end{aligned} \tag{A4}$$

(hereafter, time has been neglected for ease of notation). Similarly, the probability of detecting both particles in $x$ is given by

$$\begin{aligned}P^{(\mathrm{BOS})}(x,x)&=|\langle x,H|\langle x,V|\,|\Psi^{(+)}\rangle|^2\\&=2\,|\psi_A(x)\psi_B(y)|^2=P^{(+)}(x,x).\end{aligned} \tag{A5}$$

The same conclusions apply for fermions. Indeed in this case one has

$$\begin{aligned}P^{(\mathrm{FER})}(x,y)&=\left|\frac{[\langle x,H|\langle y,V|-\langle y,H|\langle x,V|]}{\sqrt{2}}\,|\Psi^{(-)}\rangle\right|^2\\&=|\psi_A(x)\psi_B(y)-\psi_A(y)\psi_B(x)|^2=P^{(-)}(x,y)\end{aligned} \tag{A6}$$

for $x>y$, while of course

$$P^{(\mathrm{FER})}(x,x)=0=P^{(-)}(x,x). \tag{A7}$$

A compact way to express the above quantities is by means of the symmetric version of the distributions $P^{(\pm)}(x,y)$, i.e., the quantities

$$\begin{aligned}P^{(\pm,\mathrm{sym})}(x,y)&=P^{(\pm,\mathrm{sym})}(y,x)\\&=\frac{|\psi_A(x)\psi_B(y)\pm\psi_A(y)\phi_B(x)|^2}{2}.\end{aligned} \tag{A8}$$

The functions $P^{(\pm,\mathrm{sym})}(x,y)$ are normalized when integrated over the whole domain of $x$ and $y$; i.e.,

$$\begin{aligned}\sum_{x,y}P^{(\pm,\mathrm{sym})}(x,y)&=\sum_{x,y}\frac{|\psi_A(x)\psi_B(y)\pm\psi_A(y)\psi_A(y)|^2}{2}\\&=\langle\psi_A|\psi_A\rangle\langle\psi_B|\psi_B\rangle\pm|\langle\psi_A|\psi_B\rangle|^2=1,\end{aligned} \tag{A9}$$

and possess identical marginals, i.e.,

$$\begin{aligned}P^{(\mathrm{sym})}(x)&=\sum_y P^{(\pm,\mathrm{sym})}(x,y)\\&=\frac{|\psi_A(x)|^2+|\psi_B(x)|^2}{2}\\&\quad\pm\mathrm{Re}[\psi_A(x)\psi_B(x)^*\langle\psi_B|\psi_A\rangle]\\&=\frac{|\psi_A(x)|^2+|\psi_B(x)|^2}{2}.\end{aligned} \tag{A10}$$

[Note that in writing the last identities in Eqs. (A9) and (A10) we have explicitly used the fact that $|\psi_A\rangle$ and $|\psi_B\rangle$ are orthonormal states: these vectors are in fact associated with two single-particle trajectories entering the system from two distinct ports of the interferometer.] Accordingly, we can write

$$\begin{aligned} P^{(\mathrm{BOS})}(x,y) &= 2P^{(+,\mathrm{sym})}(x,y) \qquad \text{for} \quad x > y, \\ P^{(\mathrm{BOS})}(x,x) &= P^{(+,\mathrm{sym})}(x,x) \qquad \text{for} \quad x = y, \\ P^{(\mathrm{FER})}(x,y) &= 2P^{(-,\mathrm{sym})}(x,y) \qquad \text{for} \quad x > y, \\ P^{(\mathrm{BOS})}(x,x) &= P^{(-,\mathrm{sym})}(x,x) = 0 \quad \text{for} \quad x = y. \end{aligned} \tag{A11}$$

In particular, the expectation value of any two particle observable $\Omega$ which is symmetric under particle exchange can be expressed in terms of $P^{(\pm,\mathrm{sym})}(x,y)$. Indeed, indicating by $\Omega(x,y) = \Omega(y,x)$ the spatial representation of $\Omega$, the following identity holds:

$$\begin{aligned} \langle \Omega^{(\mathrm{BOS})} \rangle &= \sum_{x \geqslant y} P^{(\mathrm{BOS})}(x,y)\Omega(x,y) \\ &= \sum_{x,y} P^{(+,\mathrm{sym})}(x,y)\Omega(x,y), \\ \langle \Omega^{(\mathrm{FER})} \rangle &= \sum_{x \geqslant y} P^{(\mathrm{FER})}(x,y)\Omega(x,y) \\ &= \sum_{x,y} P^{(-,\mathrm{sym})}(x,y)\Omega(x,y). \end{aligned} \tag{A12}$$

### 1. Single-particle detection probabilities

From the above equation one can easily compute the probability of finding a particle in position $x$. In particular, for bosons one may introduce the probability $P_{>1}^{(\mathrm{BOS})}(x)$ of finding *at least* one particle in position $x$ and the probability $P_1^{(\mathrm{BOS})}(x)$ of having *exactly* one particle in position $x$. These quantities in general differ and can be expressed as

$$\begin{aligned} &P_{>1}^{(\mathrm{BOS})}(x) \\ &= \sum_{y(<x)} P^{(\mathrm{BOS})}(x,y) + \sum_{y(>x)} P^{(\mathrm{BOS})}(y,x) + P^{(\mathrm{BOS})}(x,x) \\ &= 2\sum_{y} P^{(+,\mathrm{sym})}(x,y) - P^{(+,\mathrm{sym})}(x,x) \\ &= 2P^{(\mathrm{sym})}(x) - P^{(+,\mathrm{sym})}(x,x), \end{aligned} \tag{A13}$$

$$\begin{aligned} P_1^{(\mathrm{BOS})}(x) &= \sum_{y(<x)} P^{(\mathrm{BOS})}(x,y) + \sum_{y(>x)} P^{(\mathrm{BOS})}(y,x) \\ &= 2P^{(\mathrm{sym})}(x) - 2P^{(+,\mathrm{sym})}(x,x). \end{aligned} \tag{A14}$$

We stress that neither $P_{>1}^{(\mathrm{BOS})}(x)$ nor $P_1^{(\mathrm{BOS})}(x)$ coincides with the marginal distribution $P^{(\mathrm{sym})}(x)$ of (A10). In particular, differently from the latter, neither $P_{>1}^{(\mathrm{BOS})}(x)$ nor $P_1^{(\mathrm{BOS})}(x)$ is necessarily normalized to 1 when summing over $x$ (this is due to the fact that when summing over $x$ we are unavoidably including double-counting of events). In the fermionic case $P_{>1}^{(\mathrm{FER})}(x)$ and $P_1^{(\mathrm{FER})}(x)$ coincides due to the Pauli exclusion principle. In this case we have

$$\begin{aligned} P_1^{(\mathrm{FER})}(x) &= \sum_{y(<x)} P^{(\mathrm{FER})}(x,y) + \sum_{y(>x)} P^{(\mathrm{FER})}(y,x) \\ &= 2\sum_{y} P^{(-,\mathrm{sym})}(x,y) = 2P^{(\mathrm{sym})}(x), \end{aligned} \tag{A15}$$

which, up to a constant normalization factor, coincides with the marginal of the symmetric distribution $P^{(-,\mathrm{sym})}(x,y)$.


[1] Y. Aharonov, L. Davidovich, and N. Zagury, Phys. Rev. A **48**, 1687 (1993).

[2] M. Mohseni, P. Rebentrost, S. Lloyd, and A. Aspuru-Guzik, J. Chem. Phys. **129**, 174106 (2008).

[3] M. B. Plenio and S. F. Huelga, New J. Phys. **10**, 113019 (2008).

[4] L. Sansoni, F. Sciarrino, G. Vallone, P. Mataloni, A. Crespi, R. Ramponi, and R. Osellame, Phys. Rev. Lett. **108**, 010502 (2012).

[5] A. Peruzzo, M. Lobino, J. Matthews, N. Matsuda, A. Politi, K. Poulios, X.-Q. Zhou, Y. Lahini, N. Ismail, K. Worhoff, Y. Bromberg, Y. Silberberg, M. G. Thompson, and J. L. O'Brien, Science **329**, 1500 (2010).

[6] A. Schreiber, K.N. Cassemiro, V. Potocek, A. Gabris, P. J. Mosley, E. Andersson, I. Jex, and C. Silberhorn, Phys. Rev. Lett. **104**, 050502 (2010).

[7] A. M. Childs, Phys. Rev. Lett. **102**, 180501 (2009).

[8] A. M. Childs, D. Gosset, and Z. Webb, Science **339**, 6121 (2013).

[9] C. A. Ryan, M. Laforest, J. Boileau, and R. Laflamme, Phys. Rev. A **72**, 062317 (2005).

[10] H. Schmitz, R. Matjeschk, C. Schneider, J. Glueckert, M. Enderlein, T. Huber, and T. Schaet, Phys. Rev. Lett. **103**, 090504 (2009).

[11] F. Zähringer, G. Kirchmair, R. Gerritsma, E. Solano, R. Blatt, and C. Roos, Phys. Rev. Lett. **104**, 100503 (2010).

[12] J. Casanova, A. Mezzacapo, L. Lamata, and E. Solano, Phys. Rev. Lett. **108**, 190502 (2012).

[13] A. Mezzacapo, J. Casanova, L. Lamata, and E. Solano, Phys. Rev. Lett. **109**, 200501 (2012).

[14] P. K. Pathak and G. S. Agarwal, Phys. Rev. A **75**, 032351 (2007).

[15] A. Schreiber, K. N. Cassemiro, V. Potocek, Gabris, I. Jex, and C. Silberhorn, Phys. Rev. Lett. **106**, 180403 (2011).

[16] A. Schreiber, A. Gábris, P. P. Rohde, K. Laiho, M. Stefank, V. Potocek, C. Hamilton, I. Jex, and C. Silberhorn, Science **336**, 55 (2012).

[17] Y. Bromberg, Y. Lahini, R. Morandotti, and Y. Silberberg, Phys. Rev. Lett. **102**, 253904 (2009).

[18] J. C. F. Matthews, K. Poulios, J. D. A. Meinecke, A. Politi, A. Peruzzo, N. Ismail, K. Wörhoff, M. G. Thompson, and J. L. O'Brien, Sci. Rep. **3**, 1539 (2013).

[19] J. D. A. Meinecke, K. Poulios, A. Politi, J. C. F. Matthews, A. Peruzzo, N. Ismail, K. Wörhoff, J. L. O'Brien, and M. G. Thompson, Phys. Rev. A **88**, 012308 (2013).

[20] K. Poulios, R. Keil, D. Fry, J. D. A. Meinecke, J. C. F. Matthews, A. Politi, M. Lobino, M. Grafe, M. Heinrich, S. Nolte, A. Szameit, and J. L. O'Brien, arXiv:1308.2554v1.
[21] Y. Omar, N. Paunkovic, L. Sheridan, and S. Bose, Phys. Rev. A **74**, 042304 (2006).
[22] Y. Lahini, Y. Bromberg, D. N. Christodoulides, and Y. Silberberg, Phys. Rev. Lett. **105**, 163905 (2010).
[23] A. Crespi, R. Osellame, R. Ramponi, V. Giovannetti, R. Fazio, L. Sansoni, F. D. Nicola, F. Sciarrino, and P. Mataloni, Nature Photon. **7**, 322 (2013).
[24] C. K. Hong, Z. Y. Ou, and L. Mandel, Phys. Rev. Lett. **59**, 2044 (1987).
[25] L. Sansoni, F. Sciarrino, G. Vallone, P. Mataloni, A. Crespi, R. Ramponi, and R. Osellame, Phys. Rev. Lett. **105**, 200503 (2010).
[26] D. A. Meyer, Phys. Rev. E **55**, 5261 (1997).
[27] J. Kempe, Contemp. Phys. **44**, 307 (2003).
[28] H. Jeong, M. Paternostro, and M. S. Kim, Phys. Rev. A **69**, 012310 (2004).
[29] P. P. Rohde, A. Schreiber, M. Stefank, I. Jex, and C. Silberhorn, New J. Phys. **13**, 013001 (2011).
[30] C. Castellani, C. Di Castro, and L. Peliti, *Disordered Systems and Localization* (Springer-Verlag, Berlin, Heidelberg, 1981).
[31] P. W. Anderson, Phys. Rev. **109**, 1492 (1958).
[32] N. F. Mott, Adv. Phys. **16**, 49 (1967).
[33] P. A. Lee and T. V. Ramakrishnan, Rev. Mod. Phys. **57**, 287 (1985).
[34] I. M. Lifshits, S. A. Gredeskul, and L. A. Pastur, *Introduction to the Theory of Disordered Systems* (Wiley-Interscience, New York, 1988).
[35] C. M. Chandrashekar, arXiv:1103.2704.
[36] C.M. Chandrashekar, Phys. Rev. A **83**, 022320 (2011).
[37] A. A. Chabanov, M. Stoytchev, and A. Z. Genack, Nature **404**, 850 (2000).
[38] M. Hilke, Phys. Rev. A **80**, 063820 (2009).
[39] A. Szameit, Y. V. Kartashov, P. Zeil, F. Dreisow, M. Heinrich, R. Keil, S. Nolte, A. Tünnermann, V. A. Vysloukh, and L. Torner, Opt. Lett. **35**, 1172 (2010).
[40] S. Faez, A. Strybulevych, J. H. Page, A. Lagendijk, and B. A. van Tiggelen, Phys. Rev. Lett. **103**, 155703 (2009).
[41] S. E. Skipetrov, A. Minguzzi, B. A. van Tiggelen, and B. Shapiro, Phys. Rev. Lett. **100**, 165301 (2008).
[42] G. DiGiuseppe, L. Martin, A. Perez-Leija, R. Keil, F. Dreisow, S. Nolte, A. Szameit, A. F. Abouraddy, D. N. Christodoulides, and B. E. A. Saleh, Phys. Rev. Lett. **110**, 150503 (2013).
[43] F. W. Strauch, Phys. Rev. A **74**, 030301 (2006).
[44] V. Kendon, Math. Struct. Comput. Sci. **17**, 1169 (2006).
[45] M. A. Nielsen and I. L. Chuang, *Quantum Computation and Quantum Information* (Cambridge University Press, Cambridge, 2000).
[46] B. Aguer, S. D. Bievre, P. Lafitte, and P. E. Parris, J. Stat. Phys. **138**, 780 (2010).
[47] S. Havlin and D. B. Avraham, Adv. Phys. **51**, 187 (2002).
[48] Y. Krivolapov, L. Levi, S. Fishman, M. Segev, and M. Wilkinson, arXiv:1110.3024.
[49] B. B. Mandelbrot, *Fractal Geometry of Nature* (W.H. Freeman and Co., San Francisco, 1982), p. 402.
[50] P. G. De Gennes, La Recherche **7**, 919 (1976).
[51] J. C. Garland and D. B. Tanner, AIP Conf. Proc. **40**, 377 (1977).